Synthesis, characterization, and cytotoxic properties of mono- and di-nuclear cobalt(II)–polypridyl complexes

Article *in* Dalton Transactions · March 2018

DOI: 10.1039/C8DT00577J

CITATION
1

READS
74

5 authors, including:

Arvin Eskandari
King's College London
27 PUBLICATIONS **188** CITATIONS
SEE PROFILE

Chunxin lu
Jiaxing University
26 PUBLICATIONS **343** CITATIONS
SEE PROFILE

Sushobhan Ghosh
Gauhati University
19 PUBLICATIONS **645** CITATIONS
SEE PROFILE

Dalton Transactions

Accepted Manuscript

This article can be cited before page numbers have been issued, to do this please use: A. Eskandari, A. Kundu, C. Lu, S. Ghosh and K. Suntharalingam, *Dalton Trans.*, 2018, DOI: 10.1039/C8DT00577J.

ROYAL SOCIETY OF CHEMISTRY

rsc.li/dalton

View Article Online
DOI: 10.1039/C8DT00577J

Journal Name

ARTICLE

Synthesis, characterization, and cytotoxic properties of mono- and di-nuclear cobalt(II)-polypridyl complexes

Received 00th January 20xx,
Accepted 00th January 20xx

DOI: 10.1039/x0xx00000x

www.rsc.org/

Arvin Eskandari,[a] Arunangshu Kundu,[b] Chunxin Lu,[c] Sushobhan Ghosh,[b]* and Kogularamanan Suntharalingam[a]*

We report the synthesis and characterisation of mono- and di-nuclear cobalt(II) complexes (**1**-**3**) containing **L**[1], a polypridyl ligand with pyrazole moieties. DNA binding studies suggest that the mono-nuclear complex, **1** binds to DNA via the grooves prior to inducing oxidative DNA cleavage whereas the larger di-nuclear complexes, **2** and **3** bind to DNA via the grooves and intercalation prior to inducing oxidative DNA cleavage. The cobalt(II) complexes display micromolar potency towards U2OS (bone osteosarcoma), HepG2 (liver hepatocellular carcinoma), and GM05757 (normal human fibroblast) cells, comparable to clinically used platinum agents, cisplatin and carboplatin. Cellular mechanism of action studies shows that the most effective cobalt(II) complex, **2** enters U2OS cells, penetrates the nucleus, induces genomic DNA damage, and triggers caspase-dependent apoptosis in a p53-independent manner. This study highlights the potential of di-nuclear cobalt(II) complexes as artificial oxidative metallonucleases and tangible cancer cell-potent agents.

Introduction

Metallopharmaceuticals are among the most effective and widely used chemotherapies for treating cancer.[1,2] Platinum-based drugs such as cisplatin, carboplatin and oxaliplatin are used to treat a variety of malignancies including testicular, ovarian, lung, and colorectal cancer.[3,4] The use of these drugs is, however, limited due to acquired or inherent resistance, toxic side-effects arising from non-specificity, and their inability to prevent cancer relapse.[5-7] These drawbacks have fuelled research into developing non-platinum metal complexes with different modes of action and potentially broader spectra of activity. Several non-platinum agents have undergone preclinical investigation and even advanced clinical trials for various cancers,[8,9] however, arsenic trioxide is the only non-platinum metal complex approved for clinic use (for patients with acute promyelocytic leukaemia).[10,11] One of the major pre-clinical and clinical pitfalls confronting new anticancer metal complexes is systemic toxicity. In theory, endogenous metal-containing compounds can better mitigate this problem compared to their exogenous metal-containing counterparts (such as platinum or arsenic agents) as humans have evolved stringent pathways to overcome endogenous metal overload.[12]

Cobalt is a relatively non-toxic essential trace element metal and major component of vitamin B12 (cobalamin) and other co-enzymes.[13] An average adult human contains 1-2 mg of cobalt and absorbs 5-50 μg of cobalt daily (mainly in the form of cobalamin).[14] Given the relatively high human tolerance of cobalt, several cobalt-containing compounds have been studied for their anticancer activity over the last 35 years.[15,16] Notably, bioconjugates molecules containing cobalt(III) bis(acetylacetone)ethylenediamine and oligonucleotides were shown to inhibit transcription factors associated with cancer progression.[17-19] Cobalt(0) carbonyl-nonsteroidal anti-inflammatory drug (NSAIDs) conjugates were shown to inhibit cancer cell proliferation.[20-23] The most effective compound in this class, a $Co_2(CO)_6$ complex with an alkyne-bearing aspirin moiety (Co-ASS), is thought to induce cancer cell death via multiple mechanisms including cyclooxygenase inhibition, caspase-3 cleavage, and matrix metalloproteinase dysfunction.[24] The difference in reactivity of the accessible oxidation states of cobalt(II and III) has also enabled the development of cobalt(III) prodrugs that can undergo bioreductive activation in hypoxic regions. A number of highly promising cobalt(III) complexes with tetradentate ligands have been used to deliver therapeutic and imaging agents to hypoxic tumour microenvironments using this strategy.[25] Apart from cobalt(0) and cobalt(III) complexes, cobalt(II) complexes have also been investigated as anticancer agents albeit with limited success. Biologically active cobalt(II) complexes have been developed with Schiff base ligands, polypridyl ligands, thiosemicarbazone, and NSAIDs, however, detailed studies exploring their cellular mechanism of action are rare.[26-31] Further, very few studies are reported on the

[a] Department of Chemistry, King's College London, London, UK. E-mail: kogularamanan.suntharalingam@kcl.ac.uk
[b] Department of Chemistry, Gauhati University, Guwahati, India. E-mail: sushobhan.iisc@gmail.com
[c] Guangxi Colleges and Universities Key Laboratory of Beibu Gulf Oil and Natural Gas Resource Effective Utilization, Qinzhou University, Qinzhou 535011, China.
† Footnotes relating to the title and/or authors should appear here.
Electronic Supplementary Information (ESI) available: [details of any supplementary information available should be included here]. See DOI: 10.1039/x0xx00000x

View Article Online
DOI: 10.1039/C8DT00577J

anticancer properties of multi-nuclear cobalt(II) complexes.[32-34] Herein, we describe the synthesis, characterization, DNA binding, and antiproliferative properties of mono- and di-nuclear cobalt(II) complexes with pyrazole-based ligands and rationalize differences in their activities.

Results and discussion

Synthesis, characterisation, and lipophilicity

The mono- and di-nuclear cobalt(II) complexes, **1**-**3** were synthesised as outlined in Scheme 1 and 2. The pyrazole-based ligand, $\mathbf{L^1}$ was prepared by refluxing ortho-phenylene diamine with two equivalences of 2-(1*H*-pyrazol-1-yl)-pyridine-6-carbaldehyde[35] in dry methanol for 3 h under nitrogen. The ligand was isolated, after evaporation of the solvent, as colourless crystals in a reasonable yield (66%) and fully characterized by ^{1}H and ^{13}C NMR, infrared spectroscopy, and ESI-MS mass spectrometry (see Supporting Information). Appearance of a characteristic singlet at 6.18 ppm confirmed formation of the methylene functionality between the pyrazole and pyridine moieties. Disappearance for the aldehyde peak (ca. 10.0 ppm) associated to 2-(1*H*-pyrazol-1-yl)-pyridine-6-carbaldehyde established full conversion. The mono-nuclear cobalt(II) complex, **1** was prepared by reacting equimolar amounts of $\mathbf{L^1}$ and $Co(NO_3)_2{\cdot}6H_2O$ in dry acetonitrile for 3 h. The resultant precipitate was collected and recrystallized using methanol and diethyl ether, giving pure **1** as a deep red solid in a good yield (92%). The di-nuclear cobalt(II) complexes, **2** and **3** were prepared by reacting 4,4'-azopyridine or 4,4'-bipyridine with two equivalences of $\mathbf{L^1}$ and $Co(NO_3)_2{\cdot}6H_2O$ in dry acetonitrile for 3 h, respectively. The resultant precipitates were collected and recrystallized using methanol and diethyl ether, giving pure **2** and **3** as orange and brown solids respectively in good yields (85-88%). The cobalt(II) complexes, **1**-**3** were fully characterized by infrared spectroscopy, ESI-MS mass spectrometry, elemental analysis, and X-ray crystallography (for **1** and **3**) (see Supporting Information, CCDC 1815777 and 1815778).

Distinctive peaks corresponding to **1**-**3** with the

Scheme 1. The reaction scheme for the preparation of the mono-nuclear cobalt(II) complex, **1** containing the pyrazole-based ligand, $\mathbf{L^1}$.

appropriate isotopic pattern were observed in the ESI mass spectra (m/z = 539.0877 $[\mathbf{1}\text{-}NO_3]^+$; 1323.2311 $[\mathbf{2}\text{-}NO_3\text{-}H]^+$; 1446.9120 $[\mathbf{3}+C_4H_8O_2]^-$; Supporting Information Fig. S1-3). The purity of **1**-**3** was established by elemental analysis. Single crystals of **1** and **3** suitable for X-ray diffraction studies were obtained by slow diffusion of diethyl ether into a methanolic solution of **1** and **3** (Fig. 1 and Table S1). Both cobalt(II) complexes crystallised in the triclinic P-1 space group. Selected bond distances and bond angles data are presented in Table S2-3. The cobalt(II) centre in **1** is seven coordinate, with three bonds to nitrogen atoms on $\mathbf{L^1}$, and two bidentate interactions

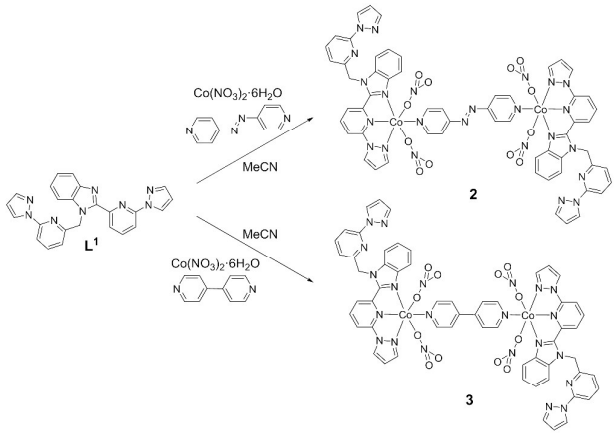

Scheme 2. The reaction scheme for the preparation of the di-nuclear cobalt(II) complexes, **2** and **3** containing the pyrazole-based ligand, $\mathbf{L^1}$ and the bridging ligands, 4,4'-azopyridine or 4,4'-bipyridine.

with nitrate ligands via the oxygen atoms. The average Co–O (2.23 Å) and Co–N (2.12 Å) bond distances are consistent with bond parameters for related heptavalent cobalt(II) complexes (Fig. 1A and S4).[36,37] The two cobalt(II) centres in the di-nuclear complex, **3** display six coordinate, distorted octahedral geometries. In each case, the equatorial plane is formed by three nitrogen atoms from $\mathbf{L^1}$ and an oxygen atom from a coordinating nitrate ligand. The axial positions are occupied by an oxygen atom from another coordinating nitrate ligand and a nitrogen atom from 4,4'-bipyridine. The average Co–O (2.11 Å) and Co–N (2.16 Å) bond distances are consistent with bond parameters for related octahedral cobalt(II) complexes (Fig. 1B and S5).[38]

The lipophilicity of **1**-**3** was determined by measuring the

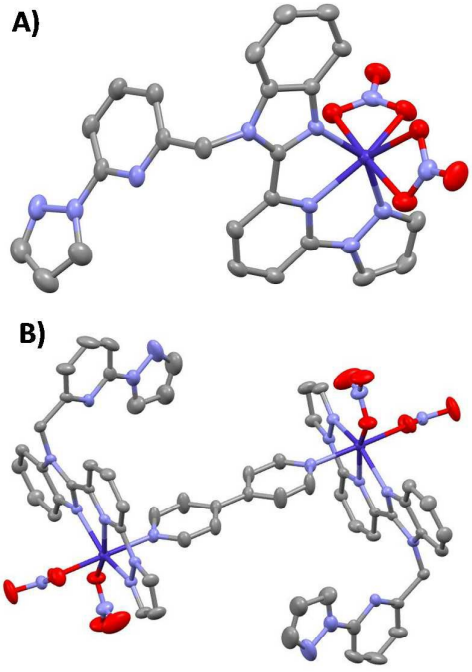

Fig. 1 X-ray structures of the cobalt(II) complexes, (A) **1** and (B) **3** comprising of the pyrazole-based ligand, $\mathbf{L^1}$. Ellipsoids are shown at 30% probability, O atoms are shown in red, C in grey, N in light blue, and Co in dark blue. H atoms have been omitted for clarity.

View Article Online
DOI: 10.1039/C8DT00577J

extent to which it partitioned between octanol and water, P. The experimentally determined LogP values varied from 0.94 ± 0.33 to 1.91 ± 0.12 (Table S4). The lipophilic nature of the complexes suggests that **1**-**3** will readily cross the phospholipid bilayer and accumulate in cells. UV-Vis and high-resolution ESI mass spectroscopy studies were carried out to assess the stability of **2**, taken as a representative member of the cobalt(II) series, in DMSO. The UV-Vis absorption of **2** (25 μM) in DMSO remained consistent over 24 h at 37 ^{o}C (Fig. S6). When dissolved in DMSO and analyzed by ESI mass spectrometry, a peak corresponding to the molecular ion of **2** with the appropriate isotopic distribution (m/z = 1323.2311, [**2**-NO_3-H]$^+$) was observed in the positive mode (Fig. S2). No significant peaks corresponding to the displacement of nitrate ligands with DMSO was observed, suggesting that **2** is reasonably stable in DMSO.

DNA cleavage and binding studies

As a number of cobalt complexes with nitrogen-coordinating ligands have been reported to bind and cleave DNA,[39-42] the DNA nuclease activity of **1**-**3** was assessed by agarose gel electrophoresis. Upon incubation of plasmid pUC19 DNA (100 ng) with **1**-**3** (0-10 μM for 16 h in the absence of external reducing agents), a modest decrease in the amount of supercoiled DNA (form I) and a simultaneous increase in the amount of nicked circular (form II) and linear (from III) DNA was observed, indicative of limited DNA cleavage (Fig. 2A and S7). The di-nuclear complex, **2** exhibited the highest nuclease activity with the appearance of linear DNA at 10 μM. In the presence of ascorbic acid (10-fold excess), **1**-**3** induced complete conversion of supercoiled DNA (form I) to nicked circular (form II) and linear DNA (form III) at 10 μM (Fig. 2B and S8). The higher nuclease activity of **1**-**3** in the presence of ascorbic acid, suggests that **1**-**3**-mediated DNA cleavage is redox-dependent. To determine the oxidative mechanism by which **1**-**3** induces DNA cleavage, nuclease activity was probed in the presence of reactive oxygen species (ROS) scavengers (NaN_3, KI, DMSO, and ^{t}BuOH) and ascorbic acid (10-fold excess) (Fig. 2C and S9). KI and NaN_3 displayed the greatest inhibitory effect, suggesting that hydrogen peroxide (H_2O_2) and singlet oxygen ($^1O_2$) are the major ROS intermediates formed during the DNA cleavage process. A similar result was previously observed for other cobalt complexes with nuclease activity.[43,44] We propose that **1**-**3** reduces molecular oxygen (in solution) to superoxide, which generates hydrogen peroxide. The paramagnetic cobalt(II) ion in **1**-**3** could be responsible for singlet oxygen generation, via a photo-redox pathway in ambient light.[45,46] To shed light on the DNA-binding mode of **1**-**3** prior to initiating DNA cleavage, the nuclease activity was probed in the presence of a minor groove binder (DAPI, 2-(4-amidinophenyl)-1H-indole-6-carboxamidine, 50 μM), a major groove binder (methyl green, 50 μM), and an intercalator (TO, thiazole orange, 10 μM). For the mono-nuclear complex, **1** DNA cleavage was inhibited in the presence of methyl green and DAPI but not TO, suggesting that **1** binds mainly via the minor and major DNA grooves (Fig. S10). For the di-nuclear complexes, **2** and **3**, DNA cleavage was inhibited in the presence of all three DNA binders suggesting that **2** and **3** binds via multiple binding sites (Fig. 2D and S10). This is reasonable considering the larger size of **2** and **3** relative to **1**.

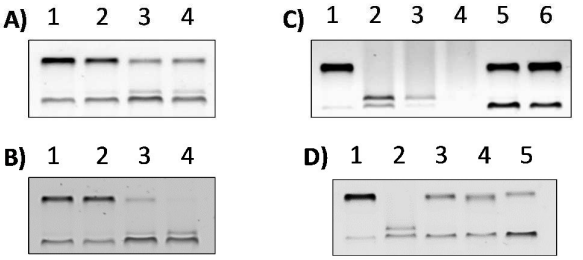

Fig. 2 DNA cleavage by **2** after a 16 h incubation period under various conditions. (A) Lane 1: DNA only; Lane 2-4: DNA + 1, 5, and 10 μM of **2**. (B) Lane 1: DNA only, Lane 2-4: DNA + 1, 5, and 10 μM of **2** with 10 equivalents of ascorbic acid. (C) Lane 1: DNA only, Lane 2: DNA + **2** (10 μM) with 10 equivalents of ascorbic acid, Lane 3-6: DNA + **2** (10 μM) with 10 equivalents of ascorbic acid + NaN_3 (40 mM), KI (40 mM), DMSO (10 mM), or ^{t}BuOH (10 mM). (D) Lane 1: DNA only, Lane 2: DNA + **2** (10 μM) with 10 equivalents of ascorbic acid, Lane 3: DNA + **2** (10 μM) with 10 equivalents of ascorbic acid + methyl green (50 μM), Lane 4: DNA + **2** (10 μM) with 10 equivalents of ascorbic acid + DAPI (50 μM), Lane 5: DNA + **2** (10 μM) with 10 equivalents of ascorbic acid + TO (10 μM).

To determine the binding affinity and further investigate the binding mode of **1**-**3** to DNA, UV-Vis spectroscopic titrations were performed. Upon addition of aliquots of calf thymus DNA (ct-DNA), in the mM range, to a solution of **1**-**3** (50 μM), significant spectral changes were observed (Fig. 3 and S11-14). The absorption band corresponding to the metal perturbed intra-ligand π-π* transition for **1** (321 nm) displayed hypochromicity (28 %), and the same band for **2** (350 nm), and **3** (353 nm) displayed hypochromicity (34-50 %) and bathochromicity (4-6 nm). These features are characteristic of interactions with DNA bases, by groove binding for **1** and both intercalation and groove binding for **2** and **3**. This is consistent with the DNA cleavage studies carried out in the presence of groove and intercalative binders (Fig. 2D and S10). From the absorbance, the concentration of bound and unbound **1**-**3** was calculated and extrapolated to determine the binding constant (Table S5).[47,48] The binding affinity (K_{bin}) of **1**-**3** to ct-DNA was calculated to be 1.42 - 4.20 × 10^5 M^{-1}. These values are up to 1 to 2 orders of magnitude lower than those reported for strong metallointercalators,[49] suggesting that non-intercalative and intercalative binding interactions could be operative.

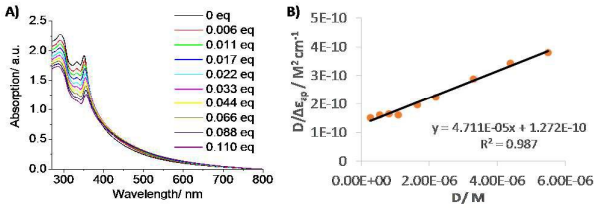

Fig. 3 (A) Representative UV-Vis trace of **2** (50 μM) upon addition of ct-DNA (0 – 0.11 equivalence). (B) Representative reciprocal plot of D/Δε$_{ap}$ versus D of **2** (50 μM) upon addition of ct-DNA (0 – 0.11 eq.).

To further probe the binding mode of **1**-**3** to DNA, ethidium bromide (a strong intercalator) displacement studies were carried out. Upon incremental addition of **1**-**3** (0 - 50

View Article Online
DOI: 10.1039/C8DT00577J

μM) to a solution of ct-DNA (20 μM) and ethidium bromide (1 μM), the emission associated to the ethidium bromide-DNA complex, originating from the intercalation of ethidium bromide between DNA base pairs, decreased to varying levels (Fig. S15-17). Upon addition of 25 μM (25 equivalences of ethidium bromide) of **1**, the emission intensity decreased by 48.1 ± 1.3 %. Under the same conditions the emission intensity decreased by 60.2 ± 1.1 % and 62.2 ± 1.4 % for **2** and **3**, respectively. A similar trend was also noted for the quenching constants (K_q) of **1**-**3**. The quenching constant of **1** (K_q = 3.11 ± 0.14 ×10^4) is significantly ($p < 0.05$) lower than that of **2** (K_q = 4.92 ± 0.29 × 10^4) and **3** (K_q = 5.27 ± 0.33 ×10^4) (Table S5). Taken together, this suggests that the **2** and **3** exhibit stronger intercalative properties than **1**. This is consistent with the DNA cleavage and UV-Vis titration data. The DNA cleavage, UV-Vis titration and ethidium displacement studies as a whole suggest that mono-nuclear complex, **1** binds to DNA via the grooves prior to inducing oxidative DNA cleavage whereas the larger di-nuclear complexes, **2** and **3** bind to DNA via the grooves as well as through intercalation prior to inducing oxidative DNA cleavage.

Cytotoxicity against cancer and normal cells

The antiproliferative effect of **1**-**3** on U2OS (bone osteosarcoma), HepG2 (liver hepatocellular carcinoma), and GM05757 (normal human fibroblast) cells was assessed using the MTT [3-(4,5-dimethylthiazol-2-yl)-2,5-diphenyltetrazolium bromide] assay. Cisplatin and carboplatin were included as a positive control. The IC_{50} values (concentrations required to decrease cell viability by 50%) were derived from dose-response curves (Fig. S18-22) and are summarized in Table 1. The cobalt(II) complexes displayed micromolar toxicities. In general, **1**-**3** were all less active than cisplatin against U2OS and HepG2 cells, and more active than carboplatin against U2OS cells (Fig. S22). The di-nuclear complexes, **2** and **3** exhibited greater potency than the mono-nuclear complex, **1**. Notably, the IC_{50} value of **3** is 2-fold lower against U2OS bone osteosarcoma cells than GM05757 normal human fibroblast cells. The 4,4'-azopyridine-containing complex, **2** displayed the highest activity across all of the cell lines tested within the cobalt(II) series. Control cytotoxicity studies showed that the potency of L^1, 4,4'-azopyridine, 4,4'-bipyridine, or $Co(NO_3)_2{\cdot}6H_2O$ towards U2OS and HepG2 cells was significantly lower than the cobalt(II) complexes, **1**-**3** (Table 1 and Fig. S23-24). This suggests that the cytotoxicity of **1**-**3** is likely to result from the intact complexes rather than their individual components (L^1, 4,4'-azopyridine, 4,4'-bipyridine, or $Co(NO_3)_2{\cdot}6H_2O$).

Table 1. IC_{50} values of **1**-**3**, L^1, 4,4'-azopyridine, 4,4'-bipyridine, $Co(NO_3)_2{\cdot}H_2O$, cisplatin, and carboplatin against U2OS, HepG2, GM07575 cells determined after 72 h incubation (mean of three independent experiments ± SD). n.d. not determined.

Compound	U2OS IC_{50} / μM	HepG2 IC_{50} / μM	GM07575 IC_{50} / μM
1	61.0 ± 8.8	81.3 ± 5.3	55.7 ± 0.9
2	37.5 ± 1.1	38.4 ± 0.8	29.1 ± 2.5
3	32.5 ± 0.6	61.6 ± 5.2	62.9 ± 5.6
L^1	109.6 ± 7.1	89.9 ± 4.5	n.d.
4,4'-azopyridine	137.6 ± 3.3	164.5 ± 4.2	n.d.
4,4'-bipyridine	142.8 ± 5.2	219.9 ± 4.2	n.d.
$Co(NO_3)_2{\cdot}6H_2O$	141.5 ± 1.1	189.9 ± 10.8	n.d.
cisplatin	13.9 ± 0.5	6.2 ± 0.1	n.d.
carboplatin	174.5 ± 8.7	33.3 ± 0.3	n.d.

Cellular mechanism of action

To determine if the cellular toxicity exhibited by the cobalt(II) complexes is related to genomic DNA damage, further cell-based studies were performed. Cell uptake studies were conducted to determine cell permeability. U2OS cells were incubated with **1**-**3** at a non-lethal dose (10 μM for 24 h) and the cobalt content was determined by inductively coupled plasma mass spectrometry (ICP-MS). As depicted in Fig. S25, the di-nuclear complexes, **2** and **3** (224.5 ± 3.6 and 214.0 ± 4.0 ppb of Co/ million cells) were taken up more readily than the

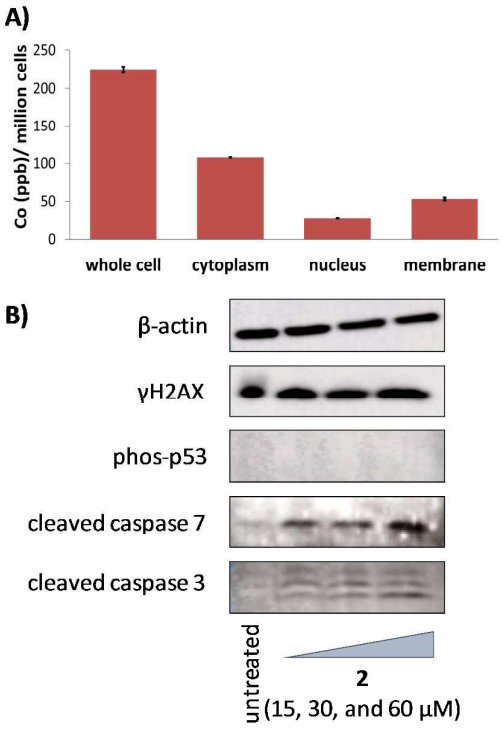

Fig. 4 (A) Cobalt content in whole cell, cytoplasm, and nucleus fractions isolated from U2OS cells treated with **2** (10 μM for 24 h). (B) Immunoblotting analysis of proteins related to the DNA damage and apoptosis pathways. Protein expression in U2OS cells following treatment with **2** (15, 30, and 60 μM) after 72 h incubation. Whole cell lysates were resolved by SDS-PAGE and analyzed by immunoblotting against γH2AX, phos-p53, cleaved caspase 7, cleaved caspase 3, and β-actin (loading control).

View Article Online
DOI: 10.1039/C8DT00577J

mono-nuclear complex, **1** (161.5 ± 2.4 ppb of Co/ million cells). Unsurprisingly, a reasonable correlation was observed between whole cell uptake, cytotoxicity (in U2OS cells), and lipophilicity. For the most cytotoxic complex, **2**, fractionation studies were carried to determine cell localization (Fig. 4A). A significant amount of **2** (12%) was detected in the nucleus, providing assess to genomic DNA. However, an appreciated amount of internalized **2** was also detected in the cytoplasm (48%) and membrane (24%) fractions, implying that **2**-mediated cell death could be related to genomic DNA-dependent or -independent mechanisms. As **2** binds and cleaves DNA (in cell-free systems) and enters the nucleus, the expression of biomarkers related to the DNA damage pathway were investigated by immunoblotting studies. DNA damage can lead to the phosphorylation of H2AX, a histone variant, at the Ser139 position by PI3K kinases.[50,51] U2OS cells treated with **2** (15-60 μM for 72 h) displayed a marked increase in expression of the phosphorylated form of H2AX (γH2AX), indicative of DNA damage (Fig. 4B). DNA damage can promote a number of chemical signals including p53 modifications. In response to DNA damage, apical kinases ATM and ATR phosphorylate p53 at the Ser15 position.[52] Incubation of U2OS cells with **2** (15-60 μM for 72 h) did not induce p53 phosphorylation (Ser15) (Fig. 4B), suggesting that **2** acts via a p53-independent pathway. Cytotoxicity studies in the presence of the p53 inhibitor, pifithrin-μ (10 μM), showed that the potency towards U2OS (IC_{50} = 25.3 ± 3.5 μM) and HepG2 (IC_{50} = 27.3 ± 4.7 μM) cells was relatively unaltered (Fig. S26-27), further suggesting that **2** induces cell death in a p53-independent fashion. Unrepaired DNA lesions can lead to apoptosis.[53] U2OS cells exposed to **2** (15-60 μM for 72 h) displayed higher levels of cleaved caspase 3 and 7 compared to untreated cells (Fig. 4B), characteristic of caspase-dependent apoptosis. Overall the cellular studies show that **2** can enter the nucleus and induces genomic DNA damage, which ultimately leads to p53-independent apoptotic cell death.

Conclusions

In summary, we report the synthesis and characterisation of mono-nuclear and di-nuclear, pyrazole-based cobalt(II) complexes with anticancer potential. The complexes, **1**-**3** display reasonable binding to DNA (1.42 - 4.20 × 10^5 M^{-1}) via the grooves and through intercalation. All complexes effectively cleave DNA through the generation of hydrogen peroxide and singlet oxygen. Interestingly, the di-nuclear complexes, **2** and **3** exhibit greater cytotoxicity than the mono-nuclear complex, **1** across a panel of two cancerous (U2OS and HepG2) and one normal (GM07575) cell lines. According to detailed mechanistic studies, the most potent complex, **2** triggers caspase-dependent apoptosis in U2OS bone osteosarcoma cells by entering the nucleus and inducing genomic DNA damage. Strikingly, **2**-mediated cell death is p53-independent. As p53 is heavily linked to tumorigenesis and is inactivated in many cancers, compound like **2** are desirable to treat p53-negative chemotherapeutic-resistant tumours. This study not only demonstrations that di-nuclear cobalt(II) complexes with pyrazole and bridging polypyridyl ligands deserve further investigation as anticancer agents capable of eliminating p53-defective cancers, but it also sheds light on cobalt-induced cell death.

Experimental

Materials and Methods. All synthetic procedures were performed under normal atmospheric conditions. ^{1}H NMR spectra were recorded on a Bruker 300 MHz NMR spectrometer. ^{1}H NMR spectra were referenced internally to residual solvent peaks, and chemical shifts are expressed relative to tetramethylsilane, $SiMe_4$ (δ = 0 ppm). Fourier transform infrared (FTIR) spectra were recorded with a IRAffinity-1S Shimadzu spectrophotometer. High resolution electron spray ionisation mass spectra were recorded on a BrukerDaltronics Esquire 3000 spectrometer by Dr. Lisa Haigh (Imperial College London). Elemental analysis of the compounds prepared was performed commercially by London Metropolitan University. 2-(1*H*-pyrazol-1-yl)-pyridine-6-carbaldehyde was prepared according to a previously reported protocol.[35]

Synthesis of L^1. In pre-dried glassware, 2-(1*H*-pyrazol-1-yl)-pyridine-6-carbaldehyde (500 mg, 3.1 mmol) and *ortho*-phenylene diamine (168 mg, 1.55 mmol) were dissolved in methanol (50 mL). The colour of the solution immediately turned dark yellow. The solution was heated under reflux for 3 h under nitrogen, resulting in a pale-yellow solution. The pale-yellow solution was filtered and the filtrate was slowly evaporated to give L^1 as colourless crystals (430 mg, 66%); ^{1}H NMR (300 MHz, $CDCl_3$): δ_H 8.52 (d, 1H), 8.41-8.39 (dd, 1H), 7.99-7.34 (m, 11H), 6.72-6.69 (d, 1H), 6.49 (d, 1H), 6.18 (s, 2H), 6.13 (d, 1H); ^{13}C NMR (300 MHz, $CDCl_3$): δ_C 155.90, 151.12, 150.63, 149.18, 148.28, 142.59, 142.28, 142.16, 139.91, 139.71, 136.79, 126.98, 124.17, 123.34, 122.10, 120.42, 117.69, 112.85, 110.96, 110.17, 107.89, 50.54; IR (KBr, cm^{-1}): 3143.97, 2954.95, 1637.56, 1575.84, 1517.98, 1467.83, 1438.90, 1392.61, 1334.74, 1256.66, 1195.87, 1143.79, 1074.35, 1039.63, 989.48, 941.26, 883.40, 823.60, 748.38, 682.80, 651.94, 615.29; ESI-MS Calcd. for $C_{24}H_{18}N_8$ $[M+H]^+$: 419.2 a.m.u. Found $[M+H]^+$: 419.6 a.m.u.

Synthesis of $Co(L^1)(NO_3)_2$ (1). In pre-dried glassware, L^1 (10 mg, 0.023 mmol) and $Co(NO_3)_2{\cdot}6H_2O$ (6.7 mg, 0.023 mmol) were stirred in dry acetonitrile (3 mL) for 3 h. This yielded a brown precipitate. The precipitate was isolated by centrifuged, and recrystallized using methanol and diethyl ether, to give **1** as a deep red solid (13 mg, 92%); HR ESI-MS Calcd. for $C_{24}H_{18}CoN_9O_3$ [**1**-NO_3]$^+$: 539.0862 a.m.u. Found [**1**-NO_3]$^+$: 539.0877 a.m.u.; IR (KBr, cm^{-1}): 3126.01, 2970.38, 2349.30, 1597.06, 1498.69, 1390.68, 1323.17, 1267.23, 1197.79, 1143.79, 1060.85, 1039.63, 941.26, 759.95, 661.58, 607.58; Anal. Calcd. for **1**, $C_{24}H_{18}CoN_{10}O_6$: C, 47.93; H, 3.02; N, 23.29. Found: C, 48.32; H, 3.12; N, 22.95.

Synthesis of $Co_2(L^1)_2(NO_3)_4$(4,4'-azopyridine) (2). In pre-dried glassware, L^1 (10 mg, 0.023 mmol), $Co(NO_3)_2{\cdot}6H_2O$ (6.7 mg, 0.023 mmol) and 4,4'-azopyridine (2.5 mg, 0.013 mmol) were stirred in dry acetonitrile (3 mL) for 3 h. This yielded an orange precipitate. The precipitate was isolated by centrifuged, and recrystallized using methanol and diethyl ether, to give **2** as an orange solid (28 mg, 85%); HR ESI-MS Calcd. for $C_{58}H_{43}Co_2N_{23}O_9$ [**2**-NO_3-H]$^+$: 1323.2264

View Article Online
DOI: 10.1039/C8DT00577J

a.m.u. Found [**2**-NO_3-H]$^+$: 1323.2311 a.m.u.; IR (KBr, cm^{-1}): 3122.75, 2951.09, 2868.15, 2355.16, 1622.13, 1602.85, 1467.83, 1408.04, 1311.59, 1124.50, 929.69, 792.74, 756.10, 659.66; Anal. Calcd. for **2**, $C_{58}H_{44}Co_2N_{24}O_{12}$: C, 50.23; H, 3.20; N, 24.24. Found: C, 50.45; H, 3.55; N, 24.35.

Synthesis of $Co_2(L^1)_2(NO_3)_4$(4,4'-bipyridine) (3). In pre-dried glassware, L^1 (10 mg, 0.023 mmol), $Co(NO_3)_2{\cdot}6H_2O$ (6.7 mg, 0.023 mmol) and 4,4'-bipyridine (2.1 mg, 0.013 mmol) were stirred in dry acetonitrile (3 mL) for 3 h. This yielded an orange precipitate. The precipitate was isolated by centrifuged, and recrystallized using methanol and diethyl ether, to give **3** as a brown solid (29 mg, 88%); HR ESI-MS Calcd. for $C_{62}H_{52}Co_2N_{22}O_{14}$ [**3**+$C_4H_8O_2$]$^-$: 1446.2681 a.m.u. Found [**3**+$C_4H_8O_2$]$^-$: 1446.9120 a.m.u.; IR (KBr, cm^{-1}): 2962.66, 2927.94, 2364.73, 1627.92, 1462.04, 1411.89, 1330.88, 1143.79, 1109.07, 993.34, 950.91, 742.59, 650.01, 607.58; Anal. Calcd. for **3**, $C_{58}H_{44}Co_2N_{22}O_{12}$: C, 51.26; H, 3.26; N, 22.68. Found: C, 51.54; H, 3.12, N, 22.43.

X-ray Single Crystal Diffraction Analysis. Standard procedures were used to mount the crystal on a Bruker Smart Apex system with graphite-monochromated Mo Kα radiation (λ = 0.71073 Å) at 293 K. The crystal structures were solved and refined using full-matrix least-squares routines, based on F^2, using SHELXL within Olex2.[54,55] All the H atoms were placed in geometrically idealised positions and constrained to ride on their parent atoms. The structures have been deposited with the Cambridge Crystallographic Data Centre (CCDC 1815777 and 1815778) and validated using *Check*CIF. This information can be obtained free of charge from www.ccdc.cam.ac.uk/data_request/cif. The Mercury software (CCDC) was used to produce the images of the structures.

DNA Cleavage Studies. Plasmid DNA (pUC19) was purchased from Invitrogen. The DNA cleavage activity of **1**-**3** was determined by monitoring the conversion of supercoiled plasmid DNA (form I) to nicked circular DNA (form II) or linear DNA (form III) in Tris-HCl buffer (5 mM, pH 7.4), using agarose-gel electrophoresis. To probe the effect of compound concentration on cleavage, solutions containing DNA (100 ng) and **1**-**3** (0-10 μM) with and without ascorbic acid (10-fold excess), with a total reaction volume of 20 μL, were incubated at 37 ^oC for 16 h. To determine the oxidative cleavage mechanism, solutions containing DNA (100 ng), **1-3** (10 μM), ascorbic acid (100 μM), and various radical scavenges (10 mM or 40 mM of KI, DMSO, ^{t}BuOH, and NaN_3), with a total reaction volume of 20 μL, were incubated at 37 ^oC for 16 h. Reactions were also conducted in the presence of methyl green (50 μM), DAPI (50 μM), and TO (10 μM). After incubation, loading buffer (5 μL, containing 0.25% bromophenol blue, 0.25% xylene cyanol, and 60% glycerol) was added and reaction mixtures were immediately loaded onto a 1% agarose gel containing ethidium bromide (1.0 mg mL^{-1}). The DNA fragments were separated by applying 60 V for 2 h in Tris-acetate EDTA (TAE) buffer. The DNA bands were analyzed under UV light using a Fujifilm Image Reader LAS-3000.

UV-Vis Tritation Studies. To determine the binding constants (K_{bin}) of **1**-**3** with ct-DNA, **1**-**3** (50 μM) was titrated with concentrated solutions of ct-DNA (mM) in Tris-HCl buffer (5 mM, pH 7.4). The binding constants were obtained by fitting the data to a reciprocal plot of $D/\Delta\varepsilon_{ap}$ versus D using the following equation: $D/\Delta\varepsilon_{ap} = D/\Delta\varepsilon - 1/(\Delta\varepsilon \times K_{bin})$ where the concentration of DNA is expressed in terms of base pairs (determined by measuring the absorption at 260 nm and the appropriate extinction coefficients) and the apparent molar extinction coefficient $\varepsilon_a = A_{observed}/[Complex]$, $\Delta\varepsilon_{ap} = [\varepsilon_a - \varepsilon_f]$ and $\Delta\varepsilon = [\varepsilon_b - \varepsilon_f]$. ε_b is the extinction coefficient of the DNA bound complex, and ε_f is the extinction coefficient of the free complex. The UV-Vis spectra were recorded on an Agilent Cary100 UV-Vis spectrophotometer. A 1 cm path- length quartz cuvette was used to carry out the measurements.

Ethidium Bromide. To a mixture of ethidium bromide (1 μM) and ct-DNA (20 μM) in Tris-HCl buffer (5 mM, pH 7.4), an increasing amount **1**-**3** (0-50 μM) was added. The emission spectrum was recorded between 550 and 800 nm with an excitation wavelength of 526 nm. The fluorescence intensity at *ca.* 608 nm was used to determine the quenching constants of **1**-**3**. The fluorescence studies were performed on a Varian Cary Eclipse spectrometer. The quenching constant (K_q) was determined using the Stern-Volmer equation: $F^o/F = K_q[Q] + 1$, where F^o is the emission intensity of ct-DNA and ethidium bromide in the absence of the cobalt(II) complexes, **1**-**3**, F is the emission intensity in the presence of the cobalt(II) complexes, **1**-**3**, K_q is the quenching constant, and [Q] is the concentration of the cobalt(II) complexes, **1**-**3**. The quenching constants were extrapolated from F^o/F versus [Q] plots.

Measurement of Water-Octanol Partition Coefficient (LogP). The LogP value for **1**-**3** was determined using the shake-flask method and UV-Vis spectroscopy. The octanol used in this experiment was pre-saturated with water. An aqueous solution of **1**-**3** (500 μL, 100 μM) was incubated with octanol (500 μL) in a 1.5 mL tube. The tube was shook at room temperature for 48 h. The two phases were separated by centrifugation and **1**-**3** content in each phase was determined by UV-Vis spectroscopy. The reported LogP values are the average of three independent experiments.

Cell Lines and Cell Culture Conditions. U2OS bone osteosarcoma, HepG2 liver hepatocellular carcinoma, and GM05757 normal human fibroblast cell lines were acquired from the American Type Culture Collection (ATCC, Manassas, VA, USA) and maintained in Dulbecco's Modified Eagle's Medium (DMEM) supplemented with 10% fetal bovine serum and 1% penicillin/streptomycin. The cells were grown at 310 K in a humidified atmosphere containing 5% CO_2.

Cytotoxicity MTT assay. The colorimetric MTT assay was used to determine the toxicity of **1**-**3**, cisplatin and carboplatin. U2OS, HepG2, or GM07575 (5×10^3) were seeded in each well of a 96-well plate. After incubating the cells overnight, various concentrations of the compounds (0.2-125 μM), were added and incubated for 72 h (total volume 200 μL). Stock solutions of the compounds were prepared as 10 mM solutions in DMSO or PBS and diluted using media. For compounds diluted from DMSO stock solutions, the final concentration of DMSO in each well was 0.5% and this amount was present in the untreated control as well. After 72 h, the medium was removed, 20 μL of a 4 mg/mL solution of MTT in PBS was added

View Article Online
DOI: 10.1039/C8DT00577J

to each well, and the plate was incubated for an additional 4 h. The DMEM/MTT mixture was aspirated and 200 µL of DMSO was added to dissolve the resulting purple formazan crystals. The absorbance of the solutions in each well was read at 550 nm. Absorbance values were normalized to (0.5% DMSO-containing) control wells and plotted as concentration of test compound versus % cell viability. The average reduction in cell viability of U2OS, HepG2, and GM07575 cells in the presence of 0.5% DMSO as opposed to no DMSO under the conditions reported was 3.3%. IC_{50} values were interpolated from the resulting dose dependent curves. The reported IC_{50} values are the average of three independent experiments, each consisting of six replicates per concentration level (overall n = 18).

Cellular Uptake. To measure the cellular uptake of **1**-**3** *ca.* 1 million U2OS cells were treated with **1**-**3** (10 µM) at 37 °C for 24 h. After incubation, the media was removed, the cells were washed with PBS (2 mL × 3), harvested, and centrifuged. The cellular pellets were dissolved in 65% HNO_3 (250 µL) overnight. For **2**, cellular pellets were also used to determine the cobalt content in the nuclear, cytoplasmic, and membrane fractions. The Thermo Scientific NE-PER Nuclear and Cytoplasmic Extraction Kit was used to extract and separate the nuclear, cytoplasmic, and membrane fractions. The fractions were dissolved in 65% HNO_3 overnight (250 µL final volume). All samples were diluted 5-fold with water and analysed using inductively coupled plasma mass spectrometry (ICP-MS, PerkinElmer NexION 350D). Cobalt levels are expressed as Co (ppb) per million cells. Results are presented as the mean of five determinations for each data point.

Immunoblotting Analysis. U2OS cells (5 x 10^5 cells) were incubated with **2** (15-60 µM for 72 h) at 37 °C. Cells were washed with PBS, scraped into SDS-PAGE loading buffer (64 mM Tris-HCl (pH 6.8)/ 9.6% glycerol/ 2% SDS/ 5% β-mercaptoethanol/ 0.01% Bromophenol Blue), and incubated at 95 °C for 10 min. Whole cell lysates were resolved by 4-20 % sodium dodecylsulphate polyacylamide gel electrophoresis (SDS-PAGE; 200 V for 25 min) followed by electro transfer to polyvinylidene difluoride membrane, PVDF (350 mA for 1 h). Membranes were blocked in 5% (w/v) non-fat milk in PBST (PBS/0.1% Tween 20) and incubated with the appropriate primary antibodies (Cell Signalling Technology). After incubation with horseradish peroxidase-conjugated secondary antibodies (Cell Signalling Technology), immune complexes were detected with the ECL detection reagent (BioRad) and analysed using a chemiluminescence imager (Amersham Imager 600).

Conflicts of interest

There are no conflicts to declare.

Acknowledgements

K.S. is supported by a Leverhulme Early Career Fellowship (ECF-2014-178). S.G. is funded by a UGC start-up grant (F.4-5/2006, BSR) and the Newton Alumni Fund. A.E. is supported by a King's College London Faculty Graduate School International Studentship. C.L. thanks the Opening Project of Guangxi Colleges and Universities Key Laboratory of Beibu Gulf Oil and Natural Gas Resource Effective Utilization (2016KL0G08) for funding. This manuscript is dedicated to Prof. Ramon Vilar for his support to K.S. and G.S.

Notes and references

1. S. P. Fricker, *Dalton Trans.*, 2007, 0, 4903-4917.
2. L. Kelland, *Nat. Rev. Cancer*, 2007, **7**, 573-584.
3. T. C. Johnstone, K. Suntharalingam and S. J. Lippard, *Chem. Rev.*, 2016, **116**, 3436-3486.
4. S. Dasari and P. B. Tchounwou, *Eur. J. Pharmacol.*, 2014, **740**, 364-378.
5. V. Brabec and J. Kasparkova, *Drug Resist. Updat.*, 2005, **8**, 131-146.
6. S. R. McWhinney, R. M. Goldberg and H. L. McLeod, *Mol. Cancer Ther.*, 2009, **8**, 10-16.
7. Z. H. Siddik, *Oncogene*, 2003, **22**, 7265-7279.
8. I. Ott and R. Gust, *Arch. Pharm.*, 2007, **340**, 117-126.
9. U. Ndagi, N. Mhlongo and M. E. Soliman, *Drug Des. Devel. Ther.*, 2017, **11**, 599-616.
10. S. L. Soignet, S. R. Frankel, D. Douer, M. S. Tallman, H. Kantarjian, E. Calleja, R. M. Stone, M. Kalaycio, D. A. Scheinberg, P. Steinherz, E. L. Sievers, S. Coutre, S. Dahlberg, R. Ellison and R. P. Warrell, Jr., *J. Clin. Oncol.*, 2001, **19**, 3852-3860.
11. K. H. Antman, *The oncologist*, 2001, **6 Suppl 2**, 1-2.
12. J. D. Donaldson and D. Beyersmann, in *Ullmann's Encyclopedia of Industrial Chemistry*, Wiley-VCH Verlag GmbH & Co. KGaA, 2000.
13. K. Yamada, in *Interrelations between Essential Metal Ions and Human Diseases*, eds. A. Sigel, H. Sigel and R. K. O. Sigel, Springer Netherlands, 2013, vol. 13, ch. 9, pp. 295-320.
14. D. Lison, in *Handbook on the Toxicology of Metals (Third Edition)*, Academic Press, Burlington, 2007, pp. 511-528.
15. M. C. Heffern, N. Yamamoto, R. J. Holbrook, A. L. Eckermann and T. J. Meade, *Curr. Opin. Chem. Biol.*, 2013, **17**, 189-196.
16. C. R. Munteanu and K. Suntharalingam, *Dalton Trans.*, 2015, **44**, 13796-13808.
17. A. S. Harney, J. Lee, L. M. Manus, P. Wang, D. M. Ballweg, C. LaBonne and T. J. Meade, *Proc. Natl. Acad. Sci. U.S.A.*, 2009, **106**, 13667-13672.
18. A. S. Harney, T. J. Meade and C. LaBonne, *PloS ONE*, 2012, **7**, e32318.
19. R. R. Hurtado, A. S. Harney, M. C. Heffern, R. J. Holbrook, R. A. Holmgren and T. J. Meade, *Mol. Pharm.*, 2012, **9**, 325-333.
20. M. Jung, D. E. Kerr and P. D. Senter, *Archiv der Pharmazie*, 1997, **330**, 173-176.
21. K. Schmidt, M. Jung, R. Keilitz, B. Schnurr and R. Gust, *Inorg. Chim. Acta.*, 2000, **306**, 6-16.
22. I. Ott, B. Kircher and R. Gust, *J. Inorg. Biochem.*, 2004, **98**, 485-489.
23. I. Ott, K. Schmidt, B. Kircher, P. Schumacher, T. Wiglenda and R. Gust, *J. Med. Chem.*, 2005, **48**, 622-629.
24. I. Ott, B. Kircher, C. P. Bagowski, D. H. Vlecken, E. B. Ott, J. Will, K. Bensdorf, W. S. Sheldrick and R. Gust, *Angew. Chem. Int. Ed.* , 2009, **48**, 1160-1163.

View Article Online
DOI: 10.1039/C8DT00577J

25. M. D. Hall, T. W. Failes, N. Yamamoto and T. W. Hambley, *Dalton Trans.*, 2007, 0, 3983-3990.
26. F. Dimiza, A. N. Papadopoulos, V. Tangoulis, V. Psycharis, C. P. Raptopoulou, D. P. Kessissoglou and G. Psomas, *Dalton Trans.*, 2010, **39**, 4517-4528.
27. F. Dimiza, A. N. Papadopoulos, V. Tangoulis, V. Psycharis, C. P. Raptopoulou, D. P. Kessissoglou and G. Psomas, *J. Inorg. Biochem.*, 2012, **107**, 54-64.
28. S. Tsiliou, L. A. Kefala, F. Perdih, I. Turel, D. P. Kessissoglou and G. Psomas, *Eur. J. Med. Chem.*, 2012, **48**, 132-142.
29. P. Martinez-Bulit, A. Garza-Ortíz, E. Mijangos, L. Barrón-Sosa, F. Sánchez-Bartéz, I. Gracia-Mora, A. Flores-Parra, R. Contreras, J. Reedijk and N. Barba-Behrens, *J. Inorg. Biochem.*, 2015, **142**, 1-7.
30. M. Sobiesiak, M. Cieslak, K. Krolewska, J. Kazmierczak-Baranska, B. Pasternak and E. Budzisz, *New J. Chem.*, 2016, **40**, 9761-9767.
31. X. Fan, J. Dong, R. Min, Y. Chen, X. Yi, J. Zhou and S. Zhang, *J. Coord. Chem.*, 2013, **66**, 4268-4279.
32. Q.-W. Huang, S.-X. Wang, S.-G. Liu, W.-Y. Su, G.-B. Li and Y.-M. He, *J. Struct. Chem.*, 2016, **57**, 188-193.
33. D.-D. Li, N. Zhang, Z.-b. Yang and Z.-W. Tao, *Appl. Organomet. Chem.*, 2017, **31**, n/a-n/a.
34. W. Zhang, D. Yao, Y. Wei, J. Tang, H. D. Bian, F. P. Huang and H. Liang, *Spectrochim Acta A Mol. Biomol. Spectrosc.*, 2016, **163**, 28-44.
35. S. Heider, H. Petzold, G. Chastanet, S. Schlamp, T. Ruffer, B. Weber and J.-F. Letard, *Dalton Trans.*, 2013, **42**, 8575-8584.
36. F. Lucarini, M. Pastore, S. Vasylevskyi, M. Varisco, E. Solari, A. Crochet, K. M. Fromm, F. Zobi and A. Ruggi, *Chem. Eur. J*, 2017, **23**, 6768-6771.
37. V. Chandrasekhar, B. Murugesa Pandian and R. Azhakar, *Polyhedron*, 2008, **27**, 255-262.
38. M. Zahedi, B. Shaabani, M. Aygün and C. Kazak, *Inorg. Chim. Acta*, 2018, **469**, 461-468.
39. M. Ahmad, M. Afzal, S. Tabassum, B. Kalinska, J. Mrozinski and P. K. Bharadwaj, *Eur. J. Med. Chem.*, 2014, **74**, 683-693.
40. S. S. Massoud, R. S. Perkins, F. R. Louka, W. Xu, A. Le Roux, Q. Dutercq, R. C. Fischer, F. A. Mautner, M. Handa, Y. Hiraoka, G. L. Kreft, T. Bortolotto and H. Terenzi, *Dalton Trans.*, 2014, **43**, 10086-10103.
41. N. Shahabadi, S. Kashanian and F. Darabi, *Eur. J. Med. Chem.*, 2010, **45**, 4239-4245.
42. W. Xu, J. A. Craft, P. R. Fontenot, M. Barens, K. D. Knierim, J. H. Albering, F. A. Mautner and S. S. Massoud, *Inorg. Chim. Acta*, 2011, **373**, 159-166.
43. P. Cressey, A. Eskandari, P. Bruno, C. Lu, M. Hemann and K. Suntharalingam, *ChemBioChem*, 2016, 17, 1713-1718.
44. P. Cressey, A. Eskandari and K. Suntharalingam, *Inorganics*, 2017, **5**, 12.
45. C. Angele-Martinez, C. Goodman and J. Brumaghim, *Metallomics*, 2014, **6**, 1358-1381.
46. S. Roy, S. Roy, S. Saha, R. Majumdar, R. R. Dighe, E. D. Jemmis and A. R. Chakravarty, *Dalton Trans.*, 2011, **40**, 1233-1242.
47. S. R. Smith, G. A. Neyhart, W. A. Kalsbeck and H. H. Thorp, *New J. Chem.*, 1994, **18**, 397-406.
48. A. Wolfe, G. H. Shimer and T. Meehan, *Biochemistry*, 1987, **26**, 6392-6396.
49. B. M. Zeglis, V. C. Pierre and J. K. Barton, *Chem. Commun.*, 2007, 0, 4565-4579.
50. S. Burma, B. P. Chen, M. Murphy, A. Kurimasa and D. J. Chen, *J. Biol. Chem.*, 2001, **276**, 42462-42467.
51. E. P. Rogakou, D. R. Pilch, A. H. Orr, V. S. Ivanova and W. M. Bonner, *J. Biol. Chem.*, 1998, **273**, 5858-5868.
52. R. S. Tibbetts, K. M. Brumbaugh, J. M. Williams, J. N. Sarkaria, W. A. Cliby, S.-Y. Shieh, Y. Taya, C. Prives and R. T. Abraham, *Genes Dev.*, 1999, **13**, 152-157.
53. W. P. Roos, A. D. Thomas and B. Kaina, *Nat. Rev. Cancer*, 2016, **16**, 20-33.
54. G. Sheldrick, *Acta Cryst.*, 2008, **A64**, 112-122.
55. O. V. Dolomanov, L. J. Bourhis, R. J. Gildea, J. A. K. Howard, H. Puschmann, *J. Appl. Cryst.*, 2009, **42**, 339-341.

View Article Online
DOI: 10.1039/C8DT00577J

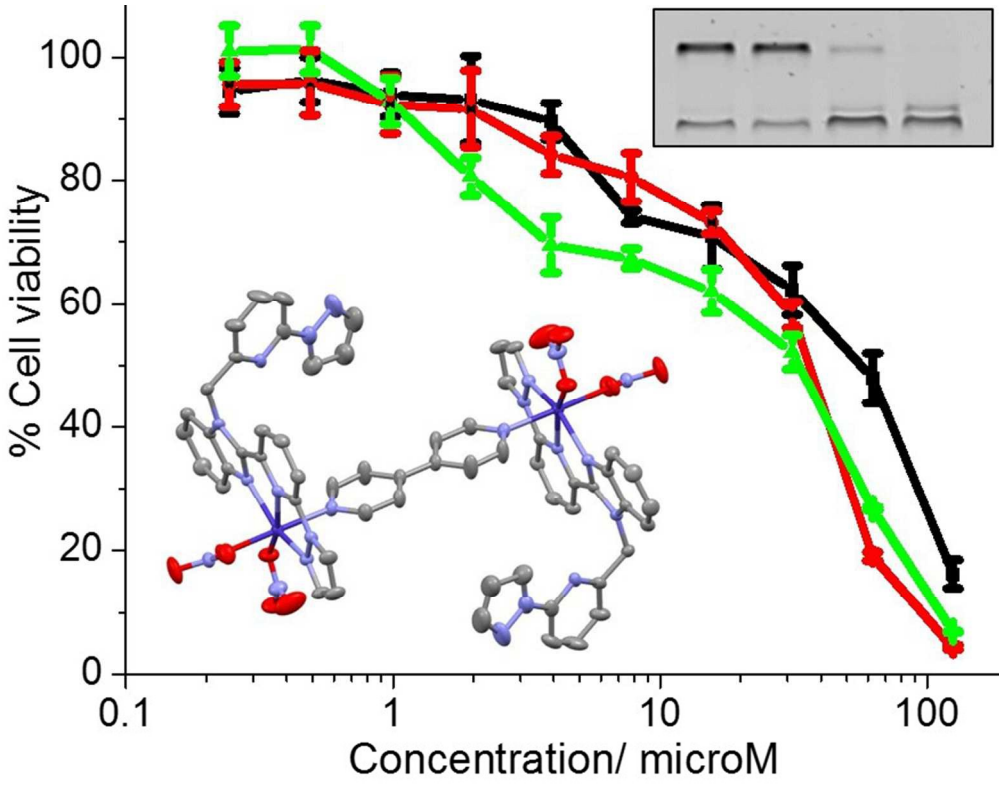

232x182mm (96 x 96 DPI)